American Journal of Advanced Research, 2020, 4-2
December. 2020, pages 17-25
doi: 10.5281/zenodo.4663485
http://www.ibii-us.org/Journals/AJAR/
ISBN 2572-8849 (Online), 2572-8830 (Print)

A review for the emerging technology of double tuned single structure MRI coil

Zongdao Li[1], Yizhen Yang[1]
[1]Departement of sciences for engineer, Sorbonne University, 4 Place Jussieu, Paris 75005, France
*Email: zong.li@etu.sorbonne-universite.fr
*Email: yizhen.yang@etu.sorbonne-universite.fr

Received on December 05, 2020; revised on December 18, 2020; published on December 30, 2020

Abstract

With the expanding accessibility of ultrahigh field MRI frameworks, researching on non-proton nuclei (X-nuclei), such as 23Na and 31P, have attracted wide attention. There are varieties of possibilities for in-depth study of this substance: firstly, it may shed light on cellular processes and energy metabolism in the field of biological tissues. Secondly, based on the first factor, it assists us to link pathological conditions to neurodegenerative diseases by displaying the nucleus. During the research, it has been found that this substance requires a well-designed radio frequency (RF) system comprising a multi-tuning RF coil. However, the intrinsic sensitivity of the aprotic nuclei is lower than 1 H, it's crucial to guarantee the signal-to-noise ratio (SNR) of the X-nuclei is as secondary as time permits. In this paper, a thorough overview of past works on configuration idea of multi-tuned coils. The primary figures of the review will be arranged into two parts: 1) State-of-the-art according to the single design structures and 2) Discussion of relevant new technologies. Further descriptions are illustrated in each subsections regarding to the detailed methodologies of dual-tuned coils, including usage of metamaterial, nested, traps and PIN-diodes, together with explanations of the novelty, best solution and trade-off.

Keywords:

1 Introduction

The advancement of ultra-high field MRI and its expanding accessibility is profitable to a number of MR research areas[1]. One rising point to advantage considerably from the expanded signal-to-noise ratio (SNR) advertised by ultra-high field systems is the examination of X-nuclei (non-proton nuclei), e.g. oxygen-17 (^{17}O), florine-19 (^{19}F), sodium-23 (^{23}Na), and phosphorus-31 (^{31}P). X-nuclei inquires about is of extraordinary intrigued as X-nuclei can be utilized to screen imperative biochemical processes and to pick up physiological data from tissues[2,3]. For case, sodium is closely included within the sodium-potassium trade handle over cell membranes and can be utilized to describe cell metabolism's features [4]. As is shown in another application, the indicator of some pathologies as well as cell viability can be provided by the values of intra and extracellular sodium concentration in tissue [5,6]. ^{31}P-MR spectroscopy got Phosphorus which is constituted by various metabolites. The investigation of these metabolites can offer some useful opinions relevant to tissue energetic and membrane metabolism [7,8]. Additionally, modifications in these metabolites are unequivocally associated with an assortment of neurotic and neurodegenerative conditions [9,10].

The reasons why studies use X-nuclei for gains in SNR are their lower MR sensitivity compared to ^1H and their substantially lower *in vivo* tissue concentration of X-nuclei. The nuclear overhauser effect can boost the SNR of quantities of ^{13}C and ^{31}P metabolites, increasing the spectral fitting accuracy as well [11,12]. Additionally, it is beneficial to acquire 1H imaging at the same time since low SNR contributes to fast scout imaging and static B_0 shimming with X-nuclei. Based on this, it is better to use multi-resonant RF coils. However, the problem is that it is quite difficult to design a ideal coil resonating at two frequencies. And compared to single-tuned coils, double-tuned coils frequently lead to low SNR. On account of this, one resonant would lose to some extent, while the other resonant frequency loses less. Based on mentioned above, to conceive a well double-tuned coil, four factors below are significant[13,14].

Although the optimum sensitivity, dependent on the purpose of use, on both the ^1H and X-nucleus channels of a dual-tuned coil is more realistic and easier than the so-called "maximum sensitivity" which requires different factors to be reckoned, it is inevitably difficult to achieve, because there will be trade-offs involved through the process of operations. However, instead, we can use single-tuned coil in order to meet a higher sensitivity and higher quality of optimization for the X-nucleus channel is restricted to ordinary experiments in a certain time, with the ^1H channel reaching the affirmable optimum sensitivity. Moreover, we may also assume by paying attention to the homogeneity or multi-tuning, so that the coil could be advanced. Decades saw the development, proposition, and demonstration of the planned applications to provide the trade-off of the best optimization.

This paper gives out an overview of the essential functions of preceding works to design multi-tuned RF coils and gives a prospect on new-developing methodologies. The single structure coil will be analyzed in the state-of-the-arts section, in which some initial concepts for each configuration, including advanced technologies for multiple tuning that include a) usage of passive components, b) usage of active switches, c) usage of geometric decoupling achievements, d) other new methods. Conference proceedings and patents, information in the form of modified and competing peer review, are also cited.

2 Single-structure

The structure initiated in this part are coils operating in a sole physical conductor at various frequencies, which is succeeded by applying different techniques. The most obvious strength of employing this method is that the single-structure can make sure the same region of imaging can be scanned and direct post-acquisition image so-registration is enabled. Additionally, the expansion of this configuration to the multiple channel array can be simply achieved by implementing isolation among the nuclei.

2.1 Trap Circuit

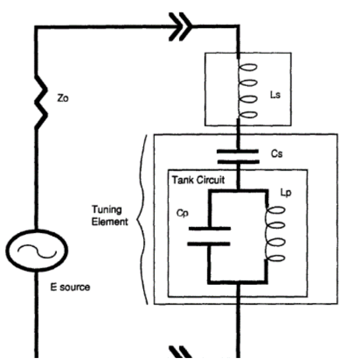

Figure 1.a The figure shows an example of a coil with two resonant frequencies using a trap circuit.[18]

The frequency splitting trap approach is conventional and commonly applied in both 1980s and 1990s [15-23]. As demonstrated in Fig.1, this trap circuit has divided one resonant frequency into two, one of which is lower and the other one is higher. By combining inductor(s) and capacitor(s), such as LC (L and C are connected in parallel) and LCC (C and L are connected in series while L is within the LC trap), the prototype of traps can be created. It is feasible to produce double or multiple resonance frequencies by placing those traps to each leg in the coil. Nonetheless, the performance and SNR of the coil will be decreased resulted from some loss caused by inserting the trap components, which can be largely attributed to the different values of inductors selected. Generally, a 25% to 30% loss rate of SNR is expected while the frequency splitting trap is compared with the single structure coil. Meantime, extent of the loss rate is controlled by adjustment of the value of inductance of trap as

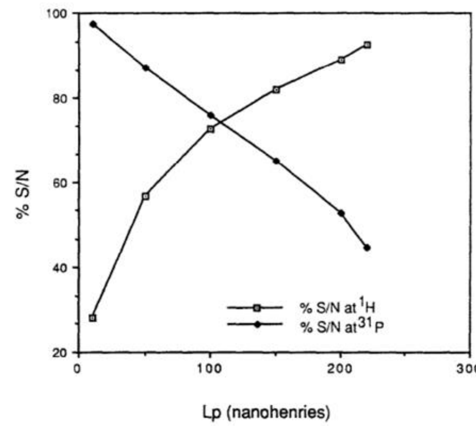

Figure 1.b This plot illustrates the influence of the trap inductor chosen at 1.5T on the SNR of 1H and 31P. [18]

displayed in Fig.1b [23]. Accordingly, the quality of the aprotic coil can be optimized by cutting down that of the ^{1}H coil.

The obvious strength of implementing this idea is that there will be no necessity to take the conflicts between ^{1}H and X-nucleus into consideration when the coil resonates at different frequencies under the same configuration. This illustrates that the B_1 field of the coil is essentially decoupled with adequate isolation among these resonant structures, which makes the process of extending the single structure coil to a multiple structure array coil easier. Nevertheless, achieving this method with close frequencies might be difficult, e.g. $^{1}H/^{19}F$ or $^{13}C/^{23}Na$.

2.2 Frequency Lock Trap Circuit

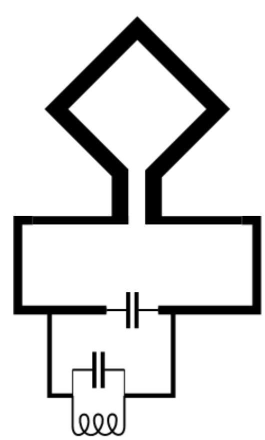

Figure 2.a Illustration of a dual-tuned antenna concept using a blocking trap to restrain 1H current flow in a portion of a single physical conductor construction or in a lumped component loop

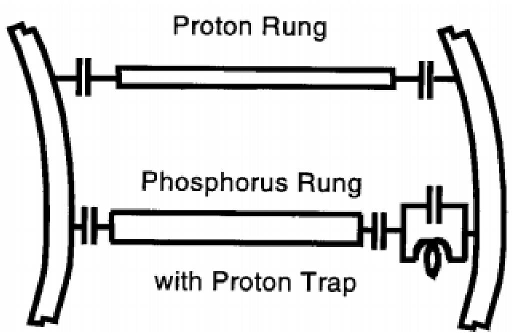

Figure 2.b It is also possible to add parallel trap circuits to each rung to filter out other frequencies, like adding a 1H blocking trap to the 31P tuning rung.

Different from splitting the resonant frequency into two, the trap can be employed to block extra frequencies in a single-tune coil [24-27] as well. Blocking efficiency, along with insertion loss, are vital elements to be taken into account when the feasibility is evaluated. With the deployment of radiation antennas, the concept of high-field application has become very prevailing.

The trap circuit can be placed in every lower frequency line of the transverse electromagnetic (TEM) type [27] coils (Fig. 2b) to avoid ^{1}H current through in the path. This idea can also be applied to the prototype design of the whole-volume birdcage coils [25] or surface coils [24], As for birdcage designs, traps are connected to each leg; lower (higher) frequency traps are attached to higher (lower) frequency rungs. Concurrently, those methods cut down the sensitivity and need to double the quantity of legs to maintain the uniformity of B_1.

2.3 Active Electronic Devices

In MRI devices, PIN-diode, as an electric control component of RF, is usually applied to manage the independent transmit and receive (T/R) coil and the active detuning units in the T/R switch [28,29]. They are employed to adjust a series of resonance frequencies to achieve dual resonances [30] as well. Majority of MRI probes are assembled with PIN-diode drivers, thus they can adequately satisfy the demand of DC bias. When a PIN-diode is operated as conductor, resistance of the diode is low in forwarding bias and high in reverse bias. Since the resistance of the PIN-diode and the noises generated (such as shot, flicker, and Johnson) [31], the sensitivity of the RF coil managed by the PIN-diode is reduced, particularly when the forward bias is taken place. From the work of Choi *et al.* [32], when PIN-diode switch (tuning on) is used, the SNR loss of one nucleus is around 35% compared with that of a single tuning reference coil. On the contrary, when it works under the reverse voltage, the loss caused by PIN-diode insertion might be ignored. Due to the reverse breakdown voltage of PIN-diode [34], the applied power is limited, which leads to the maladjustment of transmission power calibration and flip angle.

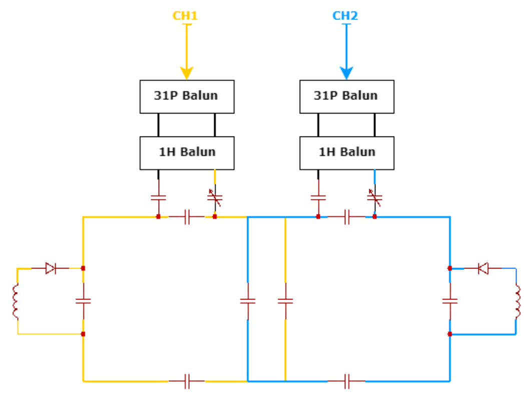

Figure 3. In combination with an inductor, that circuit can move the target resonant frequency up when positive current is supplied. A capacitor also can be substituted for the inductor to move the frequency lower.

A great many dual-tuned coils utilizing PIN-diodes were illustrated, which operate by tuning the circuit to a smaller frequency with capacitors [30, 33, 35-37] and to a larger frequency with inductors, as displayed in (Fig. 3) [32,38]. Because the Larmor frequencies of the aprotic nuclei commonly applied in MR are normally smaller than ^{1}H, the capacitors tend to be connected in series with the PIN-diodes as well as play a role in converting the tuning to the aprotic frequencies. Whereas, this becomes difficult because the X-nuclei is much less sensitive than that of the ^{1}H sensitivity, and extra losses are not expected. Thus, the latter switching method (with inductors) is preferred, supposing that the PIN-diodes will maintain power.

As a replacement to PIN-diode, varactor diode [39] as well as MEMS switch [40,41] can operate in a similar manner. In addition, the varactor diode can even control the capacitance of the tuning circuit by changing the applied voltage of the diode. In preceding work, it was used to automatically adjust and match the coil to the required conditions [42]. In spite of PIN-diodes and varactor diodes, MEMS switches are compliant with applications that require higher power.

In order to increase the capacitance on the coil, instead of using the above switch, Pratt *et al.* Has come up with a dual-tuned coil by using several manually-operated switches [43]. Even though the feasibility of the coil relies on the robustness of the physical connection in a great measure, it provides minimum coil loss and other advantages of applying dual-tuned coils, for instance, co-registration as well as shimming.

In recent years, the concept of the fluid adjustable coil has been imported, which applies a certain volume of fluid with a high dielectric constant to manage the adjusting and mapping of an MTL resonator [44]. However, in the measurement process, these procedures need to be manually operated to switch tuning.

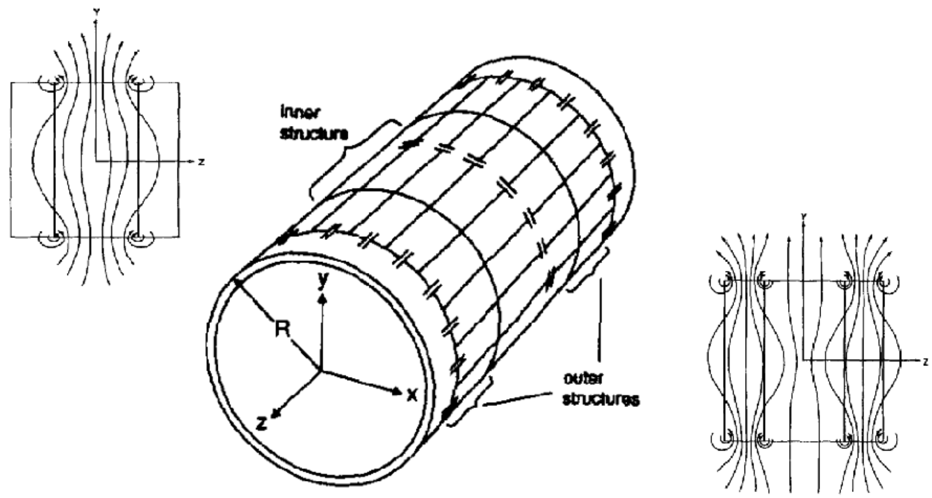

Figure 4 It is an eight legs, four end-rings birdcage with dual tuned coil. In this model, the internal structure is in low-pass configuration, which is tuned to 31P frequency (168MHz) at 9.4T, and the external structure is in high-pass, with tuning to 23Na (105.8MHz).

2.4 Different Electric Length or Intrinsically Decoupled Devices

The coil described in this section is derived from the principle that one antenna can generate multiple RF wavelengths and harmonic modes.

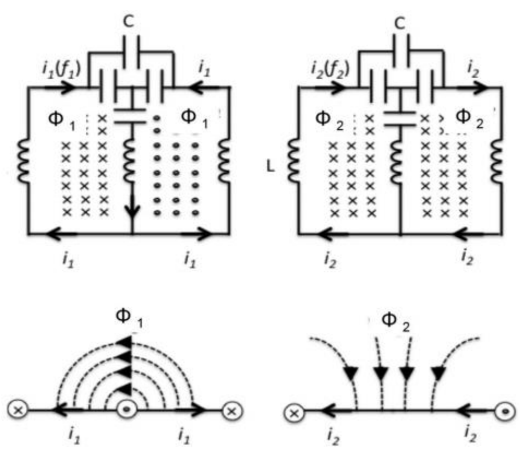

Figure 5 Because of the feedthrough approach, two differential and common mode currents can be seen to be produced. As this provides two essentially isolated B1 fields, it allows independent frequency tuning.

Surface-mode and butterfly-mode, also called common-mode and differential-mode (CMDM), volumetric [45], and surface [46] coils methods were introduced for new double-tuned coil designs. The design features two separate modes with diverse current lines in a solo design, letting the coils to operate at different value of frequencies with an inherently decoupled B1 magnetic field. For instance, in Fig. 5, the current through the two circuits flows in a figure of eight (FO8) coil configuration; generates a transverse B_1 field (in this case, common mode), while the large circle forms a single loop coil that provides a vertical B1 field for the multiple mode. The choice of these modes depends on the position of the feed point. However, in this formation, the extension of this design to volumetric or multiple channel arrays might be restricted.

Even thought the method presented above do not ask for any additional lossy electrical components to be interspersed into the probe structure, it only suitable for linear actuation. The choice to discard the data of orthogonal driving of the two nuclei with 41% SNR loss (theoretically but actually much less than this value), the reduction of RF transmit power efficiency, and the reduction of B_1 uniformity [47] in the case of the quadrature driving coil.

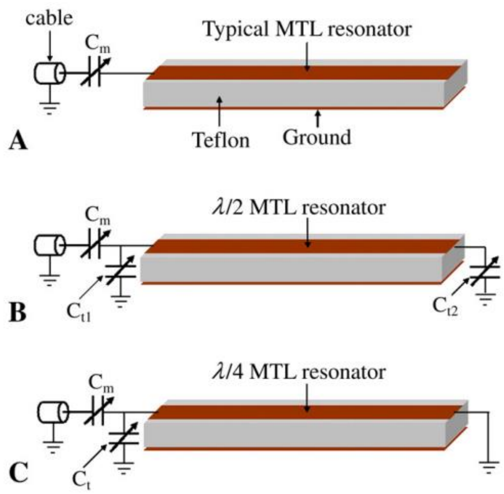

Figure 6 Schematic showing how MTL tuning at different wavelengths can finally be tuned to the individual nuclei [58].

This issue can be fixed by utilising an alternatively adjusted TEM coil [48] and a integration of λ/2 and λ/4 wavelength microstrip resonators, as displayed in Fig.6 [49]. By making use of the MTL, the wavelength of the resonator could be redesigned with the same length, which is, a λ/4 resonator with a λ/2 microstrip resonator of the same physical length can significantly reduce the operating frequency and is well suited for tuning to the X-nuclei. Thus, this volume coil is definitely able to drive the coil quadrature of both proton and aprotic channels.

Simultaneously, the results of a dual-tuned coil design according to a new multi-cellular composite right/left-handed (CRLH) metamaterial transfer wire approach have been shown. It has been demonstrated that this idea can inherently produce isomorphic current flows of two frequencies [50-52] from a common right-handed mode (parallel) and an anti-parallel left-handed mode. This resonant behavior of both frequencies is the same and the current distribution can be configured by changing the endpoint of the transmission line. For instance, to reach a λ/2 distribution, the endpoint of the lines must be short or open. The open end gives the maximum current flows in the center of the dual-tuned coil, while the short structure provides the current flows at either ends.

2.5 Four-ring Birdcage Coil

The four-ring method consists of two extra end-ring blocks on each sides of the traditional birdcage coil frame. Therefore, a single structure supporting a current division to generate a uniform RF field is modified to support two modes for spin system excitation and MR signal take in. By achieving this, the coil can be adjusted with two different frequencies, one frequency from the external and the other one from the internal.

The main mode of the inner structure is the smallest resonant frequency, while the main mode of the outer structure is the second resonant frequency, which is behind the end-ring mode. Both of them offer a homogeneous B_1 in a predetermined region of interest, including the isocenter of the coil. Some structures of four-ring birdcage can be applied, *e.g.* a low-pass for both inside and outside, or low-pass inside and high-pass outside [53]. In the study, the internal part is likely to be set on the crucial nucleus (thus, X instead of ^{1}H), while the low-pass structure is much more commonly utilized [54].

A four-ring birdcage coil is commonly used as a volume coil. An obvious strength of applying a four-ring structure is that additional lossy components are not included, thus, it retains its efficiency and sensitivity at both situations, with a loss of no more than 5% at 1.5 T [55]. In addition, it has been stated that a four-ring birdcage coil is more preferable compared with the performance of an alternate leg birdcage including traps, as it provides a higher SNR [48]. Nonetheless, this comes at the cost of inner and outer leg length ratios [56] which need to be optimized, which often leads to a significant increase in overall coil length. The accessional length demand of the outer terminal loop limits space, which can be difficult in applications using smaller coils, for instance, *in vivo* brain studies, but feasible in systemic use [57]. To avoid problems with unrealistic coil lengths, shortened and folded four ring designs were introduced [58]. Several modifications have been made to the four ring birdcage coil applying diverse coil architectures, *e.g.* Alderman-Grant coils [59], split birdcage [60], or helmet style coils [61].

3 Discussion

3.1 Minor Attenuation of Multiple Tunable Antennas

Multiple tunable radio frequency antennas are able to be designed with the emerging technologies, but the quality of Multiple tunable antennas compared to single tunable ones remains an issue. This is because the gains in one-frequency SNR *usually* worked against another. Research has shown that the by implementing geometrical decoupling, it could provide outstanding and highly efficient decoupling circuits. This practice is preferred compared to using additional lossy elements for the purpose of dual-tuning, notwithstanding the specific antenna design requirements largely depending on the use and modern application. With the developing technologies, radiating coils might be helpful for ultra-high field protium imaging, which deserved to be investigated going forward.

3.2 Dual Tunable Coils Optimized for Protium and X Cores

The quality of the 1H elements should not be ignored due to the fact that the 1H signal benefits not only scout imaging and trimming, but also functional, high-resolution and multi-parametric imaging. According to findings, a receive-only, multi-pot, dual-tuned matrix coil has been endeavored. Nonetheless, by using a traditional LC trap circuits, the coil could be enhanced by a contemporary approach.

3.3 B0 Trimming with 39Na Signal

It is not necessary to include a protium channel when the usage of 1H is only for localising images and the B0 trimming. Alternatively, B0 trimming is achievable via using non-proton signals and the most plentiful sodium signals has been applied [62]. This is favorable not only because it utilizes the high-quality single-tuned 23Na coil, but also expecting no decoupling units or complexity in the antenna structure. Furthermore, in lieu of using the 1H channel, a dual-tuned coil could be built in association with other physiologically and metabolically related nuclei, such as 23Na, 35Cl, 39K [63,64].

3.4 Simultaneous Transmission Technology

Parallel transmit (pTx) technique is now attracting more interest and is now widely used in ultrahigh field human 1H imaging. The intention is to make up for problems stemming from the shortened RF wavelength inside the tissue at higher field strength (≥ 7 T). X-nuclei Tx coils, especially for 19F imaging, could also take advantage of applying the pTx method as both professional frequencies are close together. Nevertheless, the application of pTx together with other X-nuclei is not favorable for 7T- or 9.4 T – head applications. This is evident by the fact that most MR probes up to 3 T served with a proton body antenna that produces a uniform excitation pattern, and the X-nuclei's professional frequency is either comparable or far lower than that of the 1H at 3T. However, above 9.4T, pTx could be required for 31P studies and may greatly contribute to the offer of a uniform B1 to other X-nuclei tests. Instead, the pTx technique could also help us better minimizing SAR mentioned above and make it possible for the control of independent Tx channels in the meantime. Subsequently, there are potentials where we could apply a multi-X-frequency excitation via a multiband technique and take advantage of using 31P and 23Na (or any other nuclei) excitation simultaneously. In this way, the general multinuclear MR acquisition time could be considerably shortened and the temporal resolution could be improved. What's more, pTx may also enhance the effectiveness of NOE or protium-decoupling to promote 13C and 31P measurements more thoroughly.

3.5 Novel Decoupling Solution

Decoupling between coil channels remains a crucial issue for 1H array coils and double-tuned coil designs because coil efficiency, noise, and sensitivity loss are immediately impacted by decoupling. Even though innovative decoupling schemes have been introduced recently, the three most common approaches nowadays are overlapped [65], capacitive [66], and inductive decoupling [67]. For instance, a high impedance coil design is developed by Zhang and Ruytenberg's research team with the aim to avoid the overall interactions among array elements in a phased array coil. Likewise, in order to stabilize and offset magnetic and electric coupling, there is a research team who showed a self-decoupled antenna design by modifying capacitance distribution on the coil [68]. With the implementation of these new decoupling schemes, the coil elements and their neighbours are successfully been separated, thereby the allocation of the elements in the array would be more flexible. What's more, to enhance decoupling, especially at UHF, other techniques are used, such as metamaterial-based decoupling strategy [69], induced current elimination decoupling [70], magnetic wall decoupling [71], and dense dipole arrays with split-loop resonators [72]. These methods have mostly been applied to 1H so far, yet further investigation is required regarding if these methods can be employed in the double-tuned coil and multi-channel designs.

3.6 Multimodal Dual-tuned Antennas

When dual-resonant antenna design is used together with other imaging modalities, including Linac, PET, X-ray or Ultrasound, there comes another challenge. This is due to the fact that the requirements of these modalities are absolutely different to those of MR so that hardly any traditional approach works well. Take PET as an example, coaxial cables and capacitors would result in undesired items and degradation of photon counting as the result of low-density materials within a field of view (FOV) of imaging [73]. Oehmigen*'s research team has recently introduced Hybrid MR-PET imaging* with the current design improved via total dense material relocation where most capacitors are outside the PET FOV [74]. Despite the fact that the dual-tune antenna performed much better for PET, the MRI's quality is still not desirable compared to single MRI, such as multichannel receive matrix. In addition, it is not possible to use the parallel imaging due to lacking received matrixes in the dual-tuned birdcage antenna. Therefore, this is not ideal for some studies. The effectiveness of a antenna array pattern grounded on aluminium rather than copper is examined by Anazodo *et al* [75]. Moreover, Farag and Sander's team assessed the usage of the receive matrix with PET [76]. All these activities are valuable in terms of enhancing the quality of the dual-tuned antennas when utilising for hybrid MR-PET systems.

3.7 Heating Surveillance and Specific Absorption Rate

Limited research has shown the difference of specific absorption rate (SAR) between single- and double-tuned coils. [e.g. 77, 78, 79, 80, 65] Furthermore, there is no finding on the related effect of temperature rising in the case that lumped elements are located. When concerning the general SAR performance, the finding indicates that compared to the single-tuned coil, the serious SAR penalty was not clearly shown in the double-tuned coil. However, it is strongly advised to investigate SAR or perform thermometry experiments relates to contemporary dual tunable coils.

3.8 Conclusion

The following table summarizes the dual tuning coil designs as well as the trade-offs. Note that the evaluation is to contrast the proposed dual tuning design with its corresponding single tuning coil, rather than comparison between different design approaches.

In this review, a general view of the essential parts of designing a multi-tuning RF coil is provided along with some examples of state-of-the-art techniques. Individual coils are analyzed in the state-of-the-art section where some initial concepts and multiple tuning techniques are given for each configuration, such as employing passive components, active switches, geometric decoupling techniques, etc. Finally, an outlook on emerging technologies is given as well.

Level I–V, I: Bad – V: Brilliant

APPROACH	S/N OF PROTON	S/R OF NON-PROTON X	COUPLING BETWEEN X AND ^{1}H	MULTIPLE CHANNEL EXTENDED CAPABILITY	SPATIAL LIMITATION	IMAGE JOINT REGISTRATION
TRAP	III	III	IV	V	V	V
LOCKING TRAP	IV	IV	IV	V	IV	IV
PIN-DIODE WITH CAPACITOR	V	II	V	V	IV	V
PIN-DIODE WITH INDUCTOR	II	V	V	V	IV	V
MANUAL, MECANICAL SWITCH	V	V	V	II	IV	V
FOUR-RING	IV	IV	III	N/A	II	IV
CMDM	III	III	IV	III	IV	IV
$\lambda/2$ AND $\lambda/4$ WAVELENGTH	V	V	IV	IV	III	IV
CRLH	V	V	IV	IV	III	IV

References

[1] Kraff O, Fischer A, Nagel AM, Mönninghoff C, Ladd ME.
MRI at 7 tesla and above: demonstrated and potential capabilities.
J Magn Reson Imaging 2015;41:13–33.
[2] Hu R, Kleimaier D, Malzacher M, Hoesl MAU, Paschke NK, Schad LR.
X-nuclei imaging: current state, technical challenges, and future directions.
J Magn Reson Imaging 2020;51:355–76.
[3] Niesporek SC, Nagel AM, Platt T.
Multinuclear MRI at ultrahigh fields.
Top Magn Reson Imaging 2019;28:173–88.
[4]J.P.Morth, B.P.Pedersen, M. BuchPedersen, J.P. Andersen, B. Vilsen, M.G. Palmgren, P. Nissen.
A structural overview of the plasma membrane Na+,K+-ATPase and H+-ATPase ion pumps
Nat. Rev. Mol. Cell Biol., 12 (2011), pp. 60-70
[5] Shah NJ, Worthoff WA, Langen K-J.
Imaging of sodium in the brain: a brief review.
NMR Biomed 2016;29:162–74.
[6] Madelin G, Kline R, Walvick R, Regatte RR.
A method for estimating intracellular sodium concentration and extracellular volume fraction in brain in vivo using sodium magnetic resonance imaging.
Sci Rep 2015;4:4763.
[7] de Graaf RA, Feyter HMD, Brown PB, Nixon TW, Rothman DL, Behar KL.
Detection of cerebral NAD+ in humans at 7T.
Magn Reson Med 2017;78:828–35.
[8] Detection of cerebral NAD(+) by in vivo (1)H NMR spectroscopy.
de Graaf RA, Behar KL.
NMR Biomed.
2014 Jul;27(7):802-9. doi: 10.1002/nbm.3121. Epub 2014 May 15.PMID: 24831866
[9] Stovell MG, Yan JL, Sleigh A, Mada MO, Carpenter TA, Hutchinson PJA, et al.
Assessing metabolism and injury in acute human traumatic brain injury with magnetic resonance spectroscopy: current and future applications.
Front Neurol 2017;8:642.
[10] Chouinard VA, Kim SY, Valeri L, Yuksel C, Ryan KP, Chouinard G, et al.
Brain bioenergetics and redox state measured by 31P magnetic resonance spectroscopy in unaffected siblings of patients with psychotic disorders.
Schizophr Res 2017;187:11–6.
[11] Ren J, Sherry AD, Malloy CR. Band inversion amplifies 31P–31P nuclear overhauser effects: relaxation mechanism and dynamic behavior of ATP in the human
brain by 31P MRS at 7 T. Magn Reson Med 2017;77:1409–18.
[12] Sailasuta N, Robertson LW, Harris KC, Gropman AL, Allen PS, Ross BD. Clinical
NOE 13C MRS for neuropsychiatric disorders of the frontal lobe. J Magn Reson 2008;195:219–25.
[13] Vaughan JT, Griffiths JR. RF Coils for MRI. Wiley; 2012.
[14] Felder J, Choi C-H, Shah NJ. Chapter 2: MRI Instrumentation. Hybrid MR-PET
Imaging. 2018. p. 45–63.
[15] Zakian KL, Koutcher JA, Ballon D. A dual-tuned resonator for proton-decoupled
phosphorus-31 chemical shift imaging of the brain. Magn Reson Med 1999;41:809–15.
[16] Shen GX, Boada FE, Thulborn KR. Dual-frequency, dual-quadrature, birdcage RF
coil design with identical B1 pattern for sodium and proton imaging of the human brain at 1.5 T. Magn Reson Med 1997;38:717–25.
[17] Shen GX, Wu JF, Boada FE, Thulborn KR. Experimentally verified, theoretical
Design of Dual-Tuned, low-pass birdcage radiofrequency resonators for magnetic resonance imaging and magnetic resonance spectroscopy of human brain at 3.0 tesla. Magn Reson Med 1999;41:268–75.
[18] Schnall MD, Subramanian VH, Leigh JS, Chance B. A new double-tuned probed for
concurrent 1H and 31P NMR. J Magn Reson 1985;65:122–9.
[19] Wetterling F, Tabbert M, Junge S, Gallagher L, Macrae IM, Fagan AJ. A doubletuned 1H/23Na dual resonator system for tissue sodium concentration measurements in the rat brain via Na-MRI. Phys Med Biol 2010;55:7681–95.
[20] Tadanki S, Colon RD, Moore J, Waddell KW. Double tuning a single input probe for
heteronuclear NMR spectroscopy at low field. J Magn Reson 2012;223:64–7.
[21] de Bisschop E, Annaert G, Luypaert R, Coremans J, Osteaux M. Absolute quantification of 31P muscle metabolites using NMRS with an internal standard and a high-Q, double-tuned coil. Biochim Biophys Acta 1991;1094:147–52.
[22] Leach MO, Hind A, Sauter R, Requardt H, Weber H. The design and use of a dualfrequency surface coil providing proton images for improved localization in 31P spectroscopy of small lesions. Med Phys 1986;13:510–3.
[23] Isaac G, Schnall MD, Lenkinski RE, Vogele K. A design for a double-tuned birdcage
coil for use in an integrated MRI/MRS examination. J Magn Reson 1990;89:41–50.
[24] Wetterling F, Högler M, Molkenthin U, Junge S, Gallagher L, Mhairi Macrae I, et al.
The design of a double-tuned two-port surface resonator and its application to in vivo hydrogen- and sodium-MRI. J Magn Reson 2012;217:10–8.
[25] Rath R. Design and performance of a double-tuned bird-cage coil. J Magn Reson
1990;86:488–95.
[26] Matson GB, Vermathen P, Hill TC. A practical double-tuned 1H/31P quadrature
birdcage head coil optimized for 31P operation. Magn Reson Med 1999;42:173–82.
[27] Durr W, Rauch S. A dual-frequency circularly polarizing whole-bodyMR antenna
for 69/170 MHz. Magn Reson Med 1991;19:446–55.
[28] Barberi EA, Gati JS, Rutt BK, Menon RS. A transmit-only/receive-only (TORO) RF
system for high-field MRI/MRS applications. Magn Reson Med 2000;43:284–9.
[29] Garbow JR, Mcintosh C, Conradi MS. Actively decoupled transmit–receive coilpair for mouse brain MRI. Concepts Magn Reson B 2008;33:252–9.
[30] Choi C-H, Hutchison JMS, Lurie DJ. Design and construction of an actively frequency-switchable RF coil for field-dependent magnetisation transfer contrast MRI with fast field-cycling. J Magn Reson 2010;207:134–9.
[31] Thompson M. Intuitive Analog Circuit Design. 2nd ed. Newnes; 2013.
[32] Choi C-H, Hong S, Ha Y, Shah NJ. Design and construction of a novel 1H/19F
double-tuned coil system using PIN-diode switches at 9.4T. J Magn Reson 2017;279:11–5.
[33] Lim H, Thind K, Martinez-Santiesteban FM, Scholl TJ. Construction and evaluation of a switch-tuned 13C - 1H birdcage radiofrequency coil for imaging the metabolism of hyperpolarized 13C-enriched compounds. J Magn Reson Imaging 2014;40:1082–90.
[34] Doherty W, Joos R. The PIN Diode Circuit Designers' Handbook. Watertown: Microsemi Corporation; 1998.
[35] Ha S, Hamamura MJ, Nalcioglu O, Muftuler LT. A PIN diode controlled dual-tuned
MRI RF coil and phased array for multi nuclear imaging. Phys Med Biol 2010;55:2589–600.
[36] Voelker MN, Koenig AM, Braun S, Mahnken AH, Heverhagen JT. A PIN-diodecontrolled double-tuned birdcage coil for 1H-imaging and 31P-spectroscopy on
mice. Proc Intl Soc Mag Reson Med 2013;21:2779.
[37] Han SD, Heo P, Kim HJ, Song H, Kim D, Seo J-H, et al. Double-layered dual-tuned
RF coil using frequency-selectable PIN-diode control at 7-T MRI. Concepts Magn Reson B 2017;47:e21363.
[38] Villa-Valverde P, Rodríguez I, Padró D, Benito M, Garrido-Salmon CE, Ruiz-Cabello
J. A dual 1H/19F birdcage coil for small animals at 7 T MRI. Magn Reson Mater

Phys 2019;32:79–87.

[39] Muftuler LT, Gulsen G, Sezen KD, Nalcioglu O. Automatic tuned MRI RF coil for
multinuclear imaging of small animals at 3T. J Magn Reson 2002;155:39–44.

[40] Maunder A, Rao M, Robb F, Wild JM. Comparison of MEMS switches and PIN
diodes for switched dual tuned RF coils. Magn Reson Med 2018;80:1746–53.

[41] Maunder A, Rao M, Robb F, Wild JM. An 8-element Tx/Rx array utilizing MEMS
detuning combined with 6 Rx loops for 19F and 1H lung imaging at 1.5T. Magn Reson Med 2020. https://doi.org/10.1002/mrm.28260.

[42] de Alejo RP, Garrido C, Villa P, Rodriguez I, Vaquero JJ, Ruiz-Cabello J, et al.
Automatic tuning and matching of a small multifrequency saddle coil at 4.7 T. Magn Reson Med 2004;51:869–73.

[43] Pratt R, Giaquinto R, Ireland C, et al. A novel switched frequency 3He/1H highpass birdcage coil for imaging at 1.5 tesla. Concepts Magn Reson B 2015;45:174–82.

[44] Abuelhaia A, Salma S, El-Absi M. Multi-tuned RF coil using microfluidically tunable RF

[45] Peshkovsky AS, Kennan RP, Fabry ME, Avdievich NI. Open half-volume quadrature transverse electromagnetic coil for high-field magnetic resonance imaging.
Magn Reson Med 2005;53:937–43.

[46] Pang Y, Zhang X, Xie Z, Wang C, Vigneron D. Common-mode differential-mode
(CMDM) method for double-nuclear MR signal excitation and reception at ultra-high fields. IEEE Trans Med Imaging 2011;30:1965–73.

[47] Glover GH, Hayes CE, Pelc NJ, et al. Comparison of linear and circular polarization
for magnetic resonance imaging. J Magn Reson 1985;64:255–70.

[48] Avdievich NI, Hetherington HP. Actively detuneable double-tuned 1 H/31P head
volume coil and four-channel 31P phased array for human brain spectroscopy. J Magn Reson 2007;186:341–6.

[49] Pang Y, Xie Z, Xu D, Kelley DA, Nelson SJ, Vigneron DB, et al. A dual-tuned
quadrature volume coil with mixed λ/2 and λ/4 microstrip resonators for multinuclear MRSI at 7 T. Magn Reson Imaging 2012;30:290–8.

[50] Svejda JT, Erni D, Rennings A. Near-field measurements and dual-tuned matching
of two CDRA versions for combined 1H/23Na 7 T-MRI. Proc Intl German Microwave Conf 2016:104–7.

[51] Svejda JT, Rennings A, Erni D. A metamaterial based dual-resonant coil element
for combined sodium/hydrogen MRI at 7 tesla. tm. Technisches Messen 2017;84:2–12.

[52] Svejda JT, Rennings A, Erni D. Compact metamaterial-based coil element for combined 1H/23Na MRI at 7T. Intl Conf Metamater Nanophoton 2019;4.
capacitor for RMI/MRS at 7T. IRECAP 2019;9:6.

[53] Murphy-Boesch J. Double-tuned birdcage coils: construction and tuning. Encyclop
Magn Reson 2011. https://doi.org/10.1002/9780470034590.emrstm1121.

[54] Lanz T, von Kienlin M, Behr W, Haase A. Double-tuned four-ring birdcage resonators for in vivo 31P-nuclear magnetic resonance spectroscopy at 11.75 T. Magn Reson Mat Phys Biol Med 1997;5:243–6.

[55] Murphy-Boesch J, Srinivasan R, Carvajal L, Brown TR. Two configurations of the
four-ring birdcage coil for 1 H imaging and 1 H-decoupled 31 P spectroscopy of the
human head. J Magn Reson 1994;103:103–14.

[56] Lykowsky G, Carinci F, Düring M, Weber D, Jakob PM, Haddad D. Optimization
and comparison of two practical dual-tuned birdcage configurations for quantitative assessment of articular cartilage with sodium magnetic resonance imaging.
Quant Imaging Med Surg 2015 Dec;5(6):799–805.

[57] Boskamp E, Xie Z, Taracila V, Stephen A, Edwards M, Skloss T, et al. A dual-tuned
70 cm whole-body resonator for 13C and proton MRI/MRS at 3T. Proc Intl Soc Mag Reson Med 2018;26:1714.

[58] Duan Y, Peterson BS, Liu F, Brown TR, Ibrahim TS, Kangarlu A. Computational and
experimental optimization of a double-tuned 1H/31P four-ring birdcage head coil for MRS at 3T. J Magn Reson Imaging 2009;29:13–22.

[59] Derby K, Tropp J, Hawryszko C. Design and evaluation of a novel dual-tuned resonator for spectroscopic imaging. J Magn Reson 1990;86:645–51.

[60] Potter WM, Wang L, Mccully KK, Zhao Q. Evaluation of a new 1H/31P dual-tuned
birdcage coil for 31P spectroscopy. Concepts Magn Reson B 2013;43:90–9.

[61] Hong SM, Choi C-H, Shah NJ, Felder J. Design and evaluation of a (1)H/(31)P
double-resonant helmet coil for 3T MRI of the brain. Phys Med Biol 2019;64:035003.

[62] Gast LV, Henning A, Hensel B, Uder M, Nagel AM. Localized B0 shimming based
on 23Na MRI at 7 T. Magn Reson Med 2020;83:1339–47.

[63] Nagel AM, Weber MA, Lehmann-Horn F, et al. Chlorine (35Cl) MRI in humans: clalterations do not correspond to disease-related Na+ changes. Proc Intl Soc Mag
Reson Med 2013;21:116.

[64] Umathum R, Rösler MB, Nagel AM. In vivo 39K MR imaging of human muscle and
brain. Radiology 2013;269:569–76.

[65] Roemer PR, Edelstein WA, Hayes CE, Souza SP, Mueller OM. The NMR phased
array. Mag Reson Med 1990;16:192–225.

[66] von Morze C, Tropp J, Banerjee S, Xu D, Karpodinis K, Carvajal L, et al. An eightchannel, nonoverlapping phased array coil with capacitive decoupling for parallel
MRI at 3 T. Concepts Mag Reson B 2007;31B(1):37–43.

[67] Avdievich NI, Pan JW, Hetherington HP. Resonant inductive decoupling (RID) for
transceiver arrays to compensate for both reactive and resistive components of the mutual impedance. NMR Biomed 2013;26:1547–54.

[68] Yan X, Gore JC, Grissom WA. Self-decoupled radiofrequency coils for magnetic
resonance imaging. Nat Commun 2018;9:3481.

[69] Hurshkainen AA, Derzhavskaya TA, Glybovski SB, Voogt IJ, Melchakova IV, vanden Berg CAT, et al. Element decoupling of 7T dipole body arrays by EBG metasurface structures: experimental verification. J Magn Reson 2016;269:87–96.

[70] Li Y, Xie Z, Pang Y, Vigneron D, Zhang X. ICE decoupling technique for RF coil
array designs. Med Phys 2011;38:4086–93.

[71] Yan X, Zhang X, Wei L, Xue R. Design and test of magnetic wall decoupling for
dipole transmit/receive array for MR imaging at the ultrahigh field of 7T. Appl

[72] Mollaei MSM, Hurshkainen A, Kurdjumov S, Simovski C. Double-resonant decoupling method in very dense dipole arrays. Photon Nanostruct Fundam Appl

2020;39:100767.
[73] Quick HH. Integrated PET/MR. J Magn Reson Imaging 2014;39:243–58.
[74] Oehmigen M, Lindemann ME, Gratz M, Neji R, Hammers A, Sauer M, et al. A dualtuned (13) C/(1) H head coil for PET/MR hybrid neuroimaging: development, attenuation correction, and first evaluation. Med Phys 2018;45:4877–87.
[75] Anazodo UC, Farag A, Théberg J, et al. Assessment of PET performance of a 32-channel MR brain array head coil compatible with PET for integrated PET-MRI. Proc PSMR Conf 2016.
[76] Farag A, Thompson RT, Thiessen JD, et al. Assessment of a novel 32-channel phased array for cardiovascular hybrid PET/MRI imaging: MRI performance. Eur J Hybrid Imaging 2019;3:13.
[77] Hong SM, Choi C-H, Felder J, Shah NJ. Design and simulation of dual-band dipole antenna for 1H/31P at 9.4T MRI. Proc Intl Soc Mag Reson Med 2018;26:4400.
[78] Joseph PM, Lu D. A technique for double resonant operation of birdcage imaging coils. IEEE Trans Med Imaging 1989;8:286–94.
[79] Wang C, Li Y, Wu B, Xu D, Nelson SJ, Vigneron DB, et al. A practical multinuclear transceiver volume coil for in vivo MRI/MRS at 7 T. Magn Reson Imaging 2012;30:78–84.
[80] van Uden MJ, Peeters TH, Rijpma A, Rodgers CT, Heerschap A, Scheenen TWJ. An 8-channel receive array for improved (31) P MRSI of the whole brain at 3T. Magn Reson Med 2019;82:825–32.